Chinese Journal of Aeronautics, (2022), 35(3): 390–399

Chinese Society of Aeronautics and Astronautics
& Beihang University

Chinese Journal of Aeronautics

cja@buaa.edu.cn
www.sciencedirect.com

Integrated fault estimation and fault-tolerant control for a flexible regional aircraft

Yishi LIU [a,b], **Sheng HONG** [a,*], **Enrico ZIO** [c,d,e], **Jianwei LIU** [a]

[a] *School of Cyber Science and Technology, Beihang University, Beijing 100191, China*
[b] *School of Automation Science and Electrical Engineering, Beihang University, Beijing 100191, China*
[c] *Department of Energy, Politecnico di Milano, Milano 20133, Italy*
[d] *MINES ParisTech, PSL Research University, CRC, Sophia Antipolis 06904, France*
[e] *Eminent Scholar, Department of Nuclear Engineering, College of Engineering, Kyung Hee University, Seoul 02447, South Korea*

Received 20 October 2020; revised 22 December 2020; accepted 20 February 2021
Available online 7 July 2021

KEYWORDS

Adaptive control;
Fault estimation;
Fault-tolerant control;
Flexible aircraft;
Gust load;
Integrated strategy

Abstract The article focuses on the design and application of an active reconfigurable controller that mitigates the effects of gust load and actuator faults on a flexible aircraft. A novel integrated adaptive output feedback scheme is investigated to address the actuator faults. The real-time fault values provided by the fault estimation module are considered in the reconfigurable control law to improve the fault-tolerant capability. The estimate values of faults and control gains are calculated by analyzing the stability of the overall system. The proposed controller is simulated using a flexible aircraft model with a discrete '1-cosine' gust, and the results show that it can effectively mitigate the wing root moments and recover the flight maneuver stability after the aircraft suffered from gusts.

1. Introduction

Modern aircraft become lighter and more flexible, leading to an increase in the emphasis put on atmospheric load reduction. These aircraft face two significant challenges: the pairing between rigid body and elastic modes, and the increased sensitivity to gust occurrences due to decreased wing loading and improved lift-to-drag ratios.[1] In the design of the active controller for flexible aircraft, it is important to take into account the aeroelastic effect and develop a control method capable of addressing the structural load alleviation caused by gust. A Green Regional Aircraft (GRA) with the active flight control system is modeled and analyzed in this paper. It developed by Alenia Aermacchi using Nastran and home-made tool, and both aeroelastic models and flight mechanics are considered.[2] Some control strategies were designed to decrease the effect of atmospheric perturbation using multiple control surfaces.[3] However, these control inputs may experience actuator faults in practice and the post-fault response of flexible aircraft was not considered and analyzed in the previous controller design.

Responding the problem mentioned above, Liu and his team have published a series of research works about Fault-Tolerant Control (FTC) for flexible aircraft.[4–7] The model pre-

* Corresponding author.
E-mail address: shenghong@buaa.edu.cn (S. HONG).
Peer review under responsibility of Editorial Committee of CJA.

https://doi.org/10.1016/j.cja.2021.05.025
1000-9361

dictive control, optimal control, robust control, and gain schedule method were utilized to address different actuator faults for flexible aircraft. These controllers can maintain the rigid motion of the aircraft and mitigate gust loading on the wing root in the presence of failures. Thus, it is important to take actuator faults into account for the design of controllers for flexible aircraft, because they affect the flight stability of flexible aircraft, and may generate additional structural loads and unwanted control surface oscillations. Articles about how to tackle fault effect in systems have been presented in the cited literature.[8–17] In these results, the upper bounds of fault values were used, or the fault estimation modules were regarded as a monitoring tool and were parallel-designed. However, the estimation modules interact with reconfigurable controllers and the fault signals should be regarded as a component in control laws.[18] The existing literature for the integrated design of estimation and reconfigurable control is limited. Most of works build a general linear or nonlinear system model, and design estimators and controllers by analyzing the stability of the overall system.[19–26] Many methods are used to design controllers and have a solid theoretical ground correct. However, they will fail when applied in the GRA model, because many assumptions about the rank conditions for system matrices are not satisfied and the number of unavailable state variables is large.

The objective of this article is to design an integrated fault-tolerant control scheme that control the surfaces (whether they are healthy or not) to alleviate the effect of gust or turbulence, and regain the flight maneuver stability for a flexible aircraft. Compared with the existing literature, the main contributions of the article are: (A) the fault estimation module and the reconfigurable controller are designed based on a flexible aircraft model coupling with the effect of wind gust. In Refs. 9–11, only the rigid aircraft models were considered while designing flight control systems so that these results cannot be directly used in the design of the flight control system for GRA. In Refs. 4–7, the flexible aircraft model was built to design controllers but the detrimental influences of gust were not considered; (B) the pairing between the estimation and the reconfiguration is well addressed using an integrated observer-based output feedback strategy. Comparing with Refs. 19–22, the real-time fault signals are used to design an integrated reconfigurable controller instead of the fault upper bounds.

This paper is organized as follows. An overview of the flexible aircraft model, which is used to design FTC, is given in Section 2. Section 3 gives the problem formulation, classifies actuator faults, and builds a post-fault aircraft model. The design procedure of FTC with the post-fault aircraft model is considered in Section 4. Section 5 provides the designed controller verification results. Section 6 concludes this article.

2. System modelling

The FTC system model of GRA consists of the following parts: a linearized aircraft model coupling the flight mechanics model (describes rigid body motions of the aircraft) and the aeroelastic model (describes the aircraft aeroelastic behaviour), a non-linearized actuator model with fault generator, and a fault-tolerant controller. The resulting model allows to study the flight maneuver and aeroelastic behaviour of the aircraft, when experiencing actuator faults and excited by an aerodynamic gust, and to assess the alleviation of dynamic loads through the FTC system.

2.1. State space formulation of GRA

The aim of this subsection is to give a detailed description about the state-space formulation of the GRA model. Ref. 27 reports the longitudinal equations of perturbed motion with dimensional stability derivatives, and the state vector of the rigid model is $[u_a, \alpha, \theta]^T$. Note that, the state vector of the GRA rigid model is $[x_a, z_a, \theta]^T$, which can be derived from $[u_a, \alpha, \theta]^T$, and the state vector of the elastic part is given by the modal coefficient $\boldsymbol{\eta}$. The introduction of lag terms leads to an increment in the order of the state space equation of motion and to a great number of states. In the GRA model, only one lag term (the value is 8) is used for the interpolation of unsteady aerodynamic forces.

The normal linear time-invariant GRA model (without faults) is shown as

$$\begin{cases} \dot{\boldsymbol{x}} = \boldsymbol{A}\boldsymbol{x} + \boldsymbol{B}\boldsymbol{u} + \boldsymbol{B}_g\boldsymbol{w}_g \\ \boldsymbol{y} = \boldsymbol{C}\boldsymbol{x} + \boldsymbol{D}_g\boldsymbol{w}_g \end{cases} \tag{1}$$

where $\boldsymbol{x} = \left[x_a, z_a, \theta, \boldsymbol{\eta}^T, \dot{x}_a, \dot{z}_a, \dot{\theta}, \dot{\boldsymbol{\eta}}^T, \ddot{x}_a, \ddot{z}_a, \ddot{\theta}, \ddot{\boldsymbol{\eta}}^T\right]^T$ is the state vector, $\boldsymbol{u}$ is the system input vector, $\boldsymbol{w}_g$ is the gust, $\boldsymbol{y}$ is the output vector, $\boldsymbol{A}$ is the matrix that defines the state of the model, $\boldsymbol{B}$ and $\boldsymbol{B}_g$ are the matrices that consider the effects of the system input and the gust input on the dynamic model, respectively, $\boldsymbol{C}$ is the matrix that allows to obtain physical displacement, velocities, accelerations, etc, $\boldsymbol{D}_g$ is the matrix to obtain in output the incidence angle as sum of the inertial angle of attack and the angle of attack due to the gust. The details about the unsteady aerodynamic model can be found in Ref. 28.

2.2. Gust modelling

Atmospheric disturbance models are classified into two categories: Discrete and continuous.[28] Discrete gusts are generally considered deterministic, have simple forms, and are typically treated in the time domain. This paper assumes a '1-cosine' shape for deterministic gusts and the velocity $\boldsymbol{w}_g(t)$ of the discrete gust at time t is prescribed by airworthiness regulations as

$$\boldsymbol{w}_g(t) = \frac{\boldsymbol{w}_{g0}}{2}\left(1 - \cos\frac{2\pi V_T}{L_g}t\right) \tag{2}$$

where $\boldsymbol{w}_{g0}$ is the value of the design gust velocity, V_T is the true airspeed, L_g is the gust wavelength. In the GRA model, the design gust velocity and gust wavelength are calculated as recommended by EASACS25.

2.3. Actuator fault classification

Based on the previous research, traditional aircraft actuator faults are classified into Lock-In-Place (LIP) and Loss-of-Effectiveness (LOE). With the development of the electrical flight control system, the Oscillatory Failure Case (OFC), which couples with the aeroelastic behavior of the aircraft, has become more important. In this scenario, actuator electronic components work in the fault mode and generate spuri-

ous sinusoidal signals. The detailed mathematical expressions of these fault cases are reported in Table 1. where u_i is the ith actuator output, $\boldsymbol{u}_c$ is the output vector of controllers, $\boldsymbol{L} = \mathrm{diag}\{l_1, l_2, l_3\}$ is an factors indication matrix, $l_i \in [0, 1]$, $\boldsymbol{f}_l$ and $\boldsymbol{f}_s$ are the liquid failure and solid failure, respectively.

3. Problem formulation

In this section, the general post-fault mathematical formulation of GRA, in which the system uncertainty can be summarized as an additive unknown disturbance,[29] is presented in the multiple-model formulation as

$$\begin{cases} \dot{\boldsymbol{x}} = \boldsymbol{A}\boldsymbol{x} + \boldsymbol{B}\boldsymbol{L}\boldsymbol{u} + \boldsymbol{B}\bar{\boldsymbol{f}}_a + \boldsymbol{B}_g\boldsymbol{w}_g + \boldsymbol{E}\boldsymbol{d} \\ \boldsymbol{y} = \boldsymbol{C}\boldsymbol{x} + \boldsymbol{D}_g\boldsymbol{w}_g \end{cases} \tag{3}$$

where $\bar{\boldsymbol{f}}_a = \left[\bar{f}_{a1}, \bar{f}_{a2}, \bar{f}_{a3}\right]^T$ is an additive fault value set, $\bar{f}_{ai}$ is the additive fault value of the Q actuator, $\boldsymbol{E}$ is a known matrix considering the effect of external disturbances on the dynamic model, $\boldsymbol{d}$ is the external disturbance vector.

The control objective of the investigated FTC system is to recover the rigid flight maneuver (the pitch angle, pitch rate, and angle of attack) and to mitigate the effect of gust loads acting on the wing root, i.e., the wing Root Bending Moment (RBM) and wing Root Torsional Moment (RTM) when GRA experiences gust and actuator faults. Since there is an interaction between estimation and reconfiguration, an integrated strategy is necessary and is shown in Fig. 1, where "M", "G", "A", "GRA", and "E" denote the reference model, the control gain, the actuator, the aircraft dynamics model, and the estimation, respectively. The meaning of $\boldsymbol{x}_m$, $\hat{\boldsymbol{x}}_p$, $\hat{\bar{\boldsymbol{f}}}_m$, $\hat{\bar{\boldsymbol{f}}}_a$, $\boldsymbol{u}_p$, $\boldsymbol{y}_p$ will be shown in the following section.

4. Integrated fault-tolerant control design

In this section, an integrated strategy for estimation and reconfiguration is proposed. If GRA experiences actuator faults, the system inputs cannot map the controller outputs exactly and the mismatch between them decreases the control performance of GRA or even lead to the loss of system stability. The estimation module is designed using a modified adaptive unknown input observer, which is sensitive to actuator faults and is robust to external disturbance. It gives the exact estimates of the system states, as well as fault signals. The reconfiguration module is presented using a modified adaptive control approach to recover the original system control performance and to reduce loads. Finally, the integrated strategy is used to adjust the designed system gain matrices to improve the performance and stability of the overall system.

Table 1 Classification for actuator faults.

Fault case	Mathematical expressions
Lock-in-place	$u_i = \mathrm{const}$
Loss of effectiveness	$\boldsymbol{u} = \boldsymbol{L}\boldsymbol{u}_c$
Oscillatory failure case	$\boldsymbol{u} = \boldsymbol{u}_c + \boldsymbol{f}_l$ or $\boldsymbol{u} = \boldsymbol{f}_s$

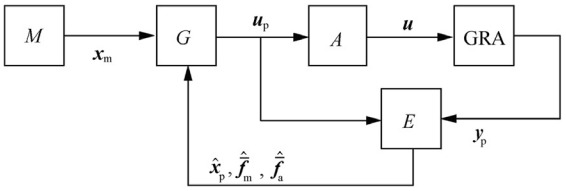

Fig. 1 Block diagram of the integrated fault-tolerant system.

4.1. Design procedure of fault estimation

In Fig. 1, the reference model contains the normal aircraft model (1) and its corresponding controller $\boldsymbol{x}_c$. An augmented system is got as

$$\begin{cases} \dot{\boldsymbol{x}}_m = \boldsymbol{A}_a\boldsymbol{x}_m + \boldsymbol{B}_a\boldsymbol{u} + \boldsymbol{B}_w\boldsymbol{w}_g + \boldsymbol{B}_r\boldsymbol{r} \\ \boldsymbol{y}_m = \boldsymbol{C}_m\boldsymbol{x}_m + \boldsymbol{D}_g\boldsymbol{w}_g \end{cases} \tag{4}$$

where $\boldsymbol{x}_m = [\boldsymbol{x}, \boldsymbol{x}_c]^T$ is the state vector of the reference model, $\boldsymbol{y}_m = \boldsymbol{y}$, $\boldsymbol{r}$ is the reference command, $\boldsymbol{A}_a = \begin{bmatrix} \boldsymbol{A} & \boldsymbol{0} \\ -\boldsymbol{C} & \boldsymbol{0} \end{bmatrix}$, $\boldsymbol{B}_a = \begin{bmatrix} \boldsymbol{B} \\ \boldsymbol{0} \end{bmatrix}$, $\boldsymbol{B}_w = \begin{bmatrix} \boldsymbol{B}_g \\ -\boldsymbol{D}_g \end{bmatrix}$, $\boldsymbol{B}_r = \begin{bmatrix} \boldsymbol{0} \\ \boldsymbol{I} \end{bmatrix}$, $\boldsymbol{C}_m = [\boldsymbol{C} \quad \boldsymbol{0}]$.

A control law $\boldsymbol{u} = \boldsymbol{G}_x\boldsymbol{x} + \boldsymbol{G}_c\boldsymbol{x}_c$ is chosen to obtain $\boldsymbol{x}_m$ and the LQR technique is used to calculate the control gains $[\boldsymbol{G}_x, \boldsymbol{G}_c] = -\boldsymbol{R}^{-1}\boldsymbol{B}_a^T\boldsymbol{P}$ where $\boldsymbol{P}$ is the solution of the Riccati Equation $\boldsymbol{P}\boldsymbol{A}_a + \boldsymbol{A}_a^T\boldsymbol{P} - \boldsymbol{P}\boldsymbol{B}_a\boldsymbol{R}^{-1}\boldsymbol{B}_a^T\boldsymbol{P} + \boldsymbol{Q} = \boldsymbol{0}$, $\boldsymbol{Q}$ and $\boldsymbol{R}$ are the designed matrices. Since the gust input $\boldsymbol{w}_g$ is an excitation for GRA, "M" is written as

$$\begin{cases} \dot{\boldsymbol{x}}_m = \boldsymbol{A}_m\boldsymbol{x}_m + \boldsymbol{B}_w\boldsymbol{w}_g + \boldsymbol{B}_r\boldsymbol{r} \\ \boldsymbol{y}_m = \boldsymbol{C}_m\boldsymbol{x}_m + \boldsymbol{D}_g\boldsymbol{w}_g \end{cases} \tag{5}$$

where $\boldsymbol{A}_m = \begin{bmatrix} \boldsymbol{A} + \boldsymbol{B}\boldsymbol{G}_x & \boldsymbol{B}\boldsymbol{G}_c \\ -\boldsymbol{C} & \boldsymbol{0} \end{bmatrix}$.

In the GRA model, the fault-tolerant controller based on the post-fault model (3) is designed to cover the performance of the normal system. Since the dimension of the post-fault model is different from the one of "M", the plant representing the post-fault model (3) and a control variable is described as

$$\begin{cases} \dot{\boldsymbol{x}}_p = \boldsymbol{A}_p\boldsymbol{x}_p + \boldsymbol{B}_p\boldsymbol{L}\boldsymbol{u}_p + \boldsymbol{B}_p\bar{\boldsymbol{f}}_a + \boldsymbol{B}_w\boldsymbol{w}_g + \boldsymbol{E}_p\boldsymbol{d} + \boldsymbol{B}_r\boldsymbol{r} \\ \boldsymbol{y}_p = \boldsymbol{C}_p\boldsymbol{x}_p + \boldsymbol{D}_g\boldsymbol{w}_g \end{cases} \tag{6}$$

where $\boldsymbol{x}_p = \begin{bmatrix} \boldsymbol{x} \\ \boldsymbol{x}_c \end{bmatrix}$, $\boldsymbol{y}_p = \boldsymbol{y}$, $\boldsymbol{A}_p = \begin{bmatrix} \boldsymbol{A} & \boldsymbol{0} \\ -\boldsymbol{C} & \boldsymbol{0} \end{bmatrix}$, $\boldsymbol{B}_p = \begin{bmatrix} \boldsymbol{B} \\ \boldsymbol{0} \end{bmatrix}$, $\boldsymbol{E}_p = \begin{bmatrix} \boldsymbol{E} \\ \boldsymbol{0} \end{bmatrix}$, $\boldsymbol{C}_p = [\boldsymbol{C}, \boldsymbol{0}]$.

The estimation module based on an adaptive observer is designed here to provide fault values as well as the estimates of the system states. The structure for observer is described as

$$\begin{cases} \dot{\boldsymbol{x}}_o = \boldsymbol{F}_o\boldsymbol{x}_o + \boldsymbol{J}_o\boldsymbol{B}_p\hat{\boldsymbol{L}}\boldsymbol{u}_p + \boldsymbol{J}_o\boldsymbol{B}_p\hat{\bar{\boldsymbol{f}}}_a + \boldsymbol{K}_o\boldsymbol{y}_p \\ \hat{\boldsymbol{x}}_p = \boldsymbol{x}_o + \boldsymbol{H}_o\boldsymbol{y}_p \end{cases} \tag{7}$$

where $\boldsymbol{x}_o$ is the observer state vector, $\hat{\boldsymbol{x}}_p$, $\hat{\boldsymbol{L}}$, and $\hat{\bar{\boldsymbol{f}}}_a$ denote the estimate value of $\boldsymbol{x}_p$, $\boldsymbol{L}$, and $\bar{\boldsymbol{f}}_a$, respectively. Matrices $\boldsymbol{F}_o$, $\boldsymbol{J}_o$, $\boldsymbol{K}_o$, and $\boldsymbol{H}_o$ are the designed observer matrices.

Theorem 1. *There exists a stable and unbiased observer (7) for the augmented post-fault system (6), if $\boldsymbol{F}_o$ is Hurwitz, the gain matrices of external excitations and uncertainty are designed to be zero, and it holds that*

$$\left(\boldsymbol{A}_p - \boldsymbol{H}_o\boldsymbol{C}_p\boldsymbol{A}_p - \boldsymbol{K}_{o1}\boldsymbol{C}_p\right) - \boldsymbol{F}_o = \boldsymbol{0} \tag{8}$$

$$\boldsymbol{F}_o\boldsymbol{H}_o - \boldsymbol{K}_{o2} = \boldsymbol{0} \tag{9}$$

$$\boldsymbol{I} - \boldsymbol{H}_o\boldsymbol{C}_p = \boldsymbol{J}_o \tag{10}$$

Proof. When the observer (7) is applied to Eq. (6), the estimate error ($\boldsymbol{e}_{po} = \boldsymbol{x}_p - \hat{\boldsymbol{x}}_p$) is governed by the following equation

$$\begin{aligned}\dot{\boldsymbol{e}}_{po} = {} & \left(\boldsymbol{A}_p - \boldsymbol{H}_o\boldsymbol{C}_p\boldsymbol{A}_p - \boldsymbol{K}_{o1}\boldsymbol{C}_p\right)\boldsymbol{e}_{po} \\ & + \left(\left(\boldsymbol{A}_p - \boldsymbol{H}_o\boldsymbol{C}_p\boldsymbol{A}_p - \boldsymbol{K}_{o1}\boldsymbol{C}_p\right) - \boldsymbol{F}_o\right)\boldsymbol{x}_o \\ & + \left(\left(\boldsymbol{A}_p - \boldsymbol{H}_o\boldsymbol{C}_p\boldsymbol{A}_p - \boldsymbol{K}_{o1}\boldsymbol{C}_p\right)\boldsymbol{H}_o - \boldsymbol{K}_{o2}\right)\boldsymbol{y}_p \\ & + \left(\left(\boldsymbol{I} - \boldsymbol{H}_o\boldsymbol{C}_p\right)\boldsymbol{B}_p\boldsymbol{L} - \boldsymbol{J}_o\boldsymbol{B}_p\hat{\boldsymbol{L}}\right)\boldsymbol{u}_p \\ & + \left(\left(\boldsymbol{I} - \boldsymbol{H}_o\boldsymbol{C}_p\right)\boldsymbol{B}_p\bar{\boldsymbol{f}}_a - \boldsymbol{J}_o\boldsymbol{B}_p\hat{\bar{\boldsymbol{f}}}_a\right) \\ & + \left(\boldsymbol{I} - \boldsymbol{H}_o\boldsymbol{C}_p\right)\boldsymbol{B}_w\boldsymbol{w}_g - \boldsymbol{H}_o\boldsymbol{D}_g\dot{\boldsymbol{w}}_g + \left(\boldsymbol{I} - \boldsymbol{H}_o\boldsymbol{C}_p\right)\boldsymbol{B}_r\boldsymbol{r} \\ & + \left(\boldsymbol{I} - \boldsymbol{H}_o\boldsymbol{C}_p\right)\boldsymbol{E}_p\boldsymbol{d}\end{aligned} \tag{11}$$

Substituting the matching conditions in Theorem 1 into Eq. (11) yields

$$\dot{\boldsymbol{e}}_{po} = \boldsymbol{F}_o\boldsymbol{e}_{po} + \boldsymbol{J}_o\boldsymbol{B}_p\left(\boldsymbol{L} - \hat{\boldsymbol{L}}\right)\boldsymbol{u}_p + \boldsymbol{J}_o\boldsymbol{B}_p\left(\bar{\boldsymbol{f}}_a - \hat{\bar{\boldsymbol{f}}}_a\right) \tag{12}$$

There are three independent control actuators in GRA so that Eq. (12) is rewritten as

$$\dot{\boldsymbol{e}}_{po} = \boldsymbol{F}_o\boldsymbol{e}_{po} + \sum_{i=1}^{3}\boldsymbol{J}_o\boldsymbol{b}_{pi}\Delta_{l_i}\boldsymbol{u}_{pi} + \sum_{i=1}^{3}\boldsymbol{J}_o\boldsymbol{b}_{pi}\Delta_{\bar{f}_{ai}} \tag{13}$$

where $\Delta_{l_i} = l_i - \hat{l}_i$ and $\Delta_{\bar{f}_{ai}} = \bar{f}_{ai} - \hat{\bar{f}}_{ai}$.

It can be concluded from Eq. (13) that if the estimate faults match to the fault descripted by the observer, i.e., $\dot{\boldsymbol{e}}_{po} = \boldsymbol{F}_o\boldsymbol{e}_{po}$, the estimate error approaches to zero asymptotically without the effect of external disturbances. This completes the proof.

Remark 1. *The designed observer provides the accurate state estimation $\hat{\boldsymbol{x}}_p$ to design the reconfiguration. Moreover, the adaptive technique is used to calculate the estimate values $\hat{\boldsymbol{L}}$ and $\hat{\bar{\boldsymbol{f}}}_a$ by analyzing the stability of the overall closed-loop system. Compared with Refs. 19–22, it removes the special assumptions for system matrices, which is not satisfied in GRA. The detailed expressions of the fault values are shown in the following integrated scheme.*

4.2. Design procedure of reconfigurable control

To control the responses of GRA tracking the states of "*M*", Eq. (6) is rewritten using the fictitious multiplicative fault formulation as

$$\begin{cases}\dot{\boldsymbol{x}}_p = \boldsymbol{A}_p\boldsymbol{x}_p + \boldsymbol{B}_p\boldsymbol{u}_p + \boldsymbol{B}_p\bar{\boldsymbol{f}}_m + \boldsymbol{B}_p\bar{\boldsymbol{f}}_a + \boldsymbol{B}_w\boldsymbol{w}_g + \boldsymbol{E}_p\boldsymbol{d} + \boldsymbol{B}_r\boldsymbol{r} \\ \boldsymbol{y}_p = \boldsymbol{C}_p\boldsymbol{x}_p + \boldsymbol{D}_g\boldsymbol{w}_g\end{cases} \tag{14}$$

where $\bar{\boldsymbol{f}}_m = \bar{\boldsymbol{L}}\boldsymbol{u}$ is the fictitious multiplicative fault value set, $\bar{\boldsymbol{L}} = \boldsymbol{L} - \boldsymbol{I} = \mathrm{diag}\left\{\bar{l}_1, \bar{l}_2, \bar{l}_3\right\}$, $\bar{l}_i \in [-1, 0]$.

Design a fault-tolerant state feedback control law as

$$\boldsymbol{u}_p = \boldsymbol{G}_e\boldsymbol{e}_{mp} + \boldsymbol{G}_m\boldsymbol{x}_m + \boldsymbol{G}_f\bar{\boldsymbol{f}}_m + \boldsymbol{G}_d \tag{15}$$

Substituting the state equations of. Eqs. (5) and (6) into the error between "*M*" and "GRA" yields

$$\begin{aligned}\dot{\boldsymbol{e}}_{mp} = {} & \left(\boldsymbol{A}_p - \boldsymbol{B}_p\boldsymbol{G}_e\right)\boldsymbol{e}_{mp} + \left(\boldsymbol{A}_m - \boldsymbol{A}_p - \boldsymbol{B}_p\boldsymbol{G}_m\right)\boldsymbol{x}_m \\ & - \left(\boldsymbol{B}_p\boldsymbol{G}_f + \boldsymbol{B}_p\right)\bar{\boldsymbol{f}}_m - \left(\boldsymbol{B}_p\boldsymbol{G}_d + \boldsymbol{B}_p\bar{\boldsymbol{f}}_a + \boldsymbol{E}_p\boldsymbol{d}\right)\end{aligned} \tag{16}$$

Design the gains to confirm that $\boldsymbol{A}_p - \boldsymbol{B}_p\boldsymbol{G}_e$ is a Hurwitz matrix, $\boldsymbol{A}_m - \boldsymbol{A}_p - \boldsymbol{B}_p\boldsymbol{G}_m = \boldsymbol{0}$, $\boldsymbol{B}_p\boldsymbol{G}_f + \boldsymbol{B}_p = \boldsymbol{0}$, and $\boldsymbol{B}_p\boldsymbol{G}_d + \boldsymbol{B}_p\bar{\boldsymbol{f}}_a + \boldsymbol{E}_p\boldsymbol{d} = \boldsymbol{0}$, so that the error tends to zero and the modeled faulty GRA follows the response of the reference model stably. However, the control gains cannot be obtained exactly because the term $\boldsymbol{E}_p\boldsymbol{d}$ is used to describe additive disturbances and different kinds of modeling uncertainties. A possible solution is to use the adaptive technique to adjust these gains.

Moreover, since the states of aeroelastic mode cannot be measured in GRA, an output feedback based fault-tolerant control law is designed as

$$\boldsymbol{u}_p = \boldsymbol{G}_y\boldsymbol{x}_m - \boldsymbol{G}_e\hat{\boldsymbol{x}}_p + \boldsymbol{G}_f\hat{\bar{\boldsymbol{f}}}_m + \boldsymbol{G}_d \tag{17}$$

where $\boldsymbol{G}_y = \boldsymbol{G}_e + \boldsymbol{G}_m$. The first derivative of the error between the plant and reference model is given as

$$\begin{aligned}\dot{\boldsymbol{e}}_{mp} = {} & \left(\boldsymbol{A}_p - \boldsymbol{B}_p\boldsymbol{G}_e\right)\boldsymbol{e}_{mp} + \left(\boldsymbol{A}_m - \boldsymbol{A}_p - \boldsymbol{B}_p\boldsymbol{G}_m\right) \\ & \boldsymbol{x}_m - \left(\boldsymbol{B}_p\boldsymbol{G}_f + \boldsymbol{B}_p\right)\hat{\bar{\boldsymbol{f}}}_m - \left(\boldsymbol{B}_p\boldsymbol{G}_d + \boldsymbol{B}_p\bar{\boldsymbol{f}}_a + \boldsymbol{E}_p\boldsymbol{d}\right) \\ & -\boldsymbol{B}_p\boldsymbol{G}_e\left(\boldsymbol{x}_p - \hat{\boldsymbol{x}}_p\right) - \boldsymbol{B}_p\left(\bar{\boldsymbol{f}}_m - \hat{\bar{\boldsymbol{f}}}_m\right)\end{aligned} \tag{18}$$

If $\hat{\boldsymbol{x}}_p$ and $\hat{\bar{\boldsymbol{f}}}_m$ approach to $\boldsymbol{x}_p$ and $\bar{\boldsymbol{f}}_m$ asymptotically, and $\boldsymbol{A}_m - \boldsymbol{A}_p - \boldsymbol{B}_p\boldsymbol{G}_m$, $\boldsymbol{B}_p\boldsymbol{G}_f + \boldsymbol{B}_p$, and $\boldsymbol{B}_p\boldsymbol{G}_d + \boldsymbol{B}_p\bar{\boldsymbol{f}}_a + \boldsymbol{E}_p\boldsymbol{d}$ tend to zero with the designed control gains, Eq. (18) can be rewritten as $\dot{\boldsymbol{e}}_{mp} = \left(\boldsymbol{A}_p - \boldsymbol{B}_p\boldsymbol{G}_e\right)\boldsymbol{e}_{mp}$. Since $\boldsymbol{A}_p - \boldsymbol{B}_p\boldsymbol{G}_e$ is Hurwitz, Eq. (18) will approach to zero asymptotically.

Remark 2. *The inaccuracy in the estimation affects the performance of the reconfiguration because the estimate state and fault values are considered in the control law (17). On the other hand, considering the error expression (11), $\boldsymbol{w}_g$ and $\boldsymbol{d}$ affect the accuracy of the estimation module. There is a bidirectional relation between the estimation and the reconfiguration, so that the separated design of them may no longer be valid.*

4.3. Integrated synthesis

To investigate the integration, the augmented closed-loop system consisting of system, controller, and observer is shown as

$$\dot{\boldsymbol{x}}_{\mathrm{p}} = \boldsymbol{A}_{\mathrm{p}}\boldsymbol{x}_{\mathrm{p}} + \boldsymbol{B}_{\mathrm{p}}\boldsymbol{u}_{\mathrm{p}} + \boldsymbol{B}_{\mathrm{p}}\bar{\boldsymbol{f}}_{\mathrm{m}} + \boldsymbol{B}_{\mathrm{p}}\bar{\boldsymbol{f}}_{\mathrm{a}} + \boldsymbol{B}_{\mathrm{w}}\boldsymbol{w}_{\mathrm{g}} + \boldsymbol{E}_{\mathrm{p}}\boldsymbol{d} + \boldsymbol{B}_{\mathrm{r}}\boldsymbol{r} \tag{19a}$$

$$\begin{aligned}\dot{\boldsymbol{e}}_{\mathrm{mp}} = {} & (\boldsymbol{A}_{\mathrm{p}} - \boldsymbol{B}_{\mathrm{p}}\boldsymbol{G}_{\mathrm{e}})\boldsymbol{e}_{\mathrm{mp}} + (\boldsymbol{A}_{\mathrm{m}} - \boldsymbol{A}_{\mathrm{p}} - \boldsymbol{B}_{\mathrm{p}}\boldsymbol{G}_{\mathrm{m}})\boldsymbol{x}_{\mathrm{m}} - (\boldsymbol{B}_{\mathrm{p}}\boldsymbol{G}_{\mathrm{f}} + \boldsymbol{B}_{\mathrm{p}})\hat{\bar{\boldsymbol{f}}}_{\mathrm{m}} \\ & - \left(\boldsymbol{B}_{\mathrm{p}}\boldsymbol{G}_{\mathrm{d}} + \boldsymbol{B}_{\mathrm{p}}\bar{\boldsymbol{f}}_{\mathrm{a}} + \boldsymbol{E}_{\mathrm{p}}\boldsymbol{d}\right) - \boldsymbol{B}_{\mathrm{p}}\boldsymbol{G}_{\mathrm{e}}(\boldsymbol{x}_{\mathrm{p}} - \hat{\boldsymbol{x}}_{\mathrm{p}}) - \boldsymbol{B}_{\mathrm{p}}\left(\bar{\boldsymbol{f}}_{\mathrm{m}} - \hat{\bar{\boldsymbol{f}}}_{\mathrm{m}}\right)\end{aligned} \tag{19b}$$

$$\dot{\boldsymbol{e}}_{\mathrm{po}} = \boldsymbol{F}_{\mathrm{o}}\boldsymbol{e}_{\mathrm{po}} + \boldsymbol{J}_{\mathrm{o}}\boldsymbol{B}_{\mathrm{p}}\left(\boldsymbol{L} - \hat{\boldsymbol{L}}\right)\boldsymbol{u}_{\mathrm{p}} + \boldsymbol{J}_{\mathrm{o}}\boldsymbol{B}_{\mathrm{p}}\left(\bar{\boldsymbol{f}}_{\mathrm{a}} - \hat{\bar{\boldsymbol{f}}}_{\mathrm{a}}\right) \tag{19c}$$

$$\boldsymbol{y}_{\mathrm{p}} = \boldsymbol{C}_{\mathrm{p}}\boldsymbol{x}_{\mathrm{p}} + \boldsymbol{D}_{\mathrm{g}}\boldsymbol{w}_{\mathrm{g}} \tag{19d}$$

Theorem 2. *The asymptotic stability of the augmented closed-loop system* (19) *is guaranteed, if the estimate faults and control gains satisfied the following conditions*

$$\hat{l}_i(t) = \int_0^t \alpha_i \boldsymbol{e}_{\mathrm{po}}^{\mathrm{T}}\boldsymbol{P}_{\mathrm{po}}\boldsymbol{J}\boldsymbol{b}_{\mathrm{p}i}\boldsymbol{u}_{\mathrm{p}i}\mathrm{d}\tau + \hat{l}_i(0) \tag{20}$$

$$\hat{\bar{f}}_{ai}(t) = \int_0^t \beta_i \boldsymbol{e}_{\mathrm{po}}^{\mathrm{T}}\boldsymbol{P}_{\mathrm{po}}\boldsymbol{J}\boldsymbol{b}_{\mathrm{p}i}\mathrm{d}\tau + \hat{\bar{f}}_{ai}(0) \tag{21}$$

where $\hat{l}_i(0) = 0$ and $\hat{\bar{f}}_{ai}(0) = 0$ are the initial values and

$$\boldsymbol{G}_{\mathrm{e}}(t) = \int_o^t \left(\boldsymbol{e}_{\mathrm{mp}}\boldsymbol{e}_{\mathrm{mp}}^{\mathrm{T}}\boldsymbol{P}_{\mathrm{mp}}\boldsymbol{B}_{\mathrm{p}}\boldsymbol{\Phi}_1^{-1}\right)^{\mathrm{T}}\mathrm{d}\tau + \boldsymbol{G}_{\mathrm{e}}(0) \tag{22}$$

$$\boldsymbol{G}_{\mathrm{m}}(t) = \int_o^t \left(\boldsymbol{x}_{\mathrm{m}}\boldsymbol{e}_{\mathrm{mp}}^{\mathrm{T}}\boldsymbol{P}_{\mathrm{mp}}\boldsymbol{B}_{\mathrm{p}}\boldsymbol{\Phi}_2^{-1}\right)^{\mathrm{T}}\mathrm{d}\tau + \boldsymbol{G}_{\mathrm{m}}(0) \tag{23}$$

$$\boldsymbol{G}_{\mathrm{f}}(t) = \int_o^t \left(\bar{\boldsymbol{f}}_{\mathrm{m}}\boldsymbol{e}_{\mathrm{mp}}^{\mathrm{T}}\boldsymbol{P}_{\mathrm{mp}}\boldsymbol{B}_{\mathrm{p}}\boldsymbol{\Phi}_3^{-1}\right)^{\mathrm{T}}\mathrm{d}\tau + \boldsymbol{G}_{\mathrm{f}}(0) \tag{24}$$

$$\boldsymbol{G}_{\mathrm{d}}(t) = \int_o^t \left(\boldsymbol{e}_{\mathrm{mp}}^{\mathrm{T}}\boldsymbol{P}_{\mathrm{mp}}\boldsymbol{B}_{\mathrm{p}}\boldsymbol{\Phi}_4^{-1}\right)^{\mathrm{T}}\mathrm{d}\tau + \boldsymbol{G}_{\mathrm{d}}(0) \tag{25}$$

where $\boldsymbol{G}_{\mathrm{e}}(0) = \boldsymbol{B}_{\mathrm{p}}^{\dagger}(\boldsymbol{A}_{\mathrm{p}} - \boldsymbol{A}_{\mathrm{pH}})$, $\boldsymbol{G}_{\mathrm{m}}(0) = \boldsymbol{B}_{\mathrm{p}}^{\dagger}(\boldsymbol{A}_{\mathrm{m}} - \boldsymbol{A}_{\mathrm{p}})$, $\boldsymbol{G}_{\mathrm{f}}(0) = -\boldsymbol{B}_{\mathrm{p}}^{\dagger}\boldsymbol{B}_{\mathrm{p}}$, and $\boldsymbol{G}_{\mathrm{d}}(0) = 0$ are initial values. $\boldsymbol{A}_{\mathrm{pH}}$ is a designed Hurwitz matrix and $\boldsymbol{B}_{\mathrm{p}}^{\dagger}$ is the pseudo-inverse of $\boldsymbol{B}_{\mathrm{p}}$.

Proof. Because of the pairing between the estimation and reconfiguration, the observer and controller are integrated design by analyzing the stability of the overall system (19). $\boldsymbol{G}_{\mathrm{e}}$, $\boldsymbol{G}_{\mathrm{m}}$, $\boldsymbol{G}_{\mathrm{f}}$, and $\boldsymbol{G}_{\mathrm{d}}$ are classical state feedback gain matrices and from such viewpoint, Eq. (16) is rewritten as

$$\begin{aligned}\dot{\boldsymbol{e}}_{\mathrm{mp}} = {} & \left(\boldsymbol{A}_{\mathrm{pH}} + \boldsymbol{B}_{\mathrm{p}}\boldsymbol{G}_{\mathrm{e}}(0) - \boldsymbol{B}_{\mathrm{p}}\boldsymbol{G}_{\mathrm{e}}(t)\right)\boldsymbol{e}_{\mathrm{mp}} \\ & + \left(\boldsymbol{B}_{\mathrm{p}}\boldsymbol{G}_{\mathrm{m}}(0) - \boldsymbol{B}_{\mathrm{p}}\boldsymbol{G}_{\mathrm{m}}(t)\right)\boldsymbol{x}_{\mathrm{m}} - \left(\boldsymbol{B}_{\mathrm{p}}\boldsymbol{G}_{\mathrm{f}}(t) - \boldsymbol{B}_{\mathrm{p}}\boldsymbol{G}_{\mathrm{f}}(0)\right)\bar{\boldsymbol{f}}_{\mathrm{m}} \\ & - \left(\boldsymbol{B}_{\mathrm{p}}\boldsymbol{G}_{\mathrm{d}}(t) - \boldsymbol{B}_{\mathrm{p}}\boldsymbol{G}_{\mathrm{d}}(0)\right) = \boldsymbol{A}_{\mathrm{pH}}\boldsymbol{e}_{\mathrm{mp}} - \boldsymbol{B}_{\mathrm{p}}\boldsymbol{\Gamma}_1\boldsymbol{e}_{\mathrm{mp}} \\ & - \boldsymbol{B}_{\mathrm{p}}\boldsymbol{\Gamma}_2\boldsymbol{x}_{\mathrm{m}} - \boldsymbol{B}_{\mathrm{p}}\boldsymbol{\Gamma}_3\bar{\boldsymbol{f}}_{\mathrm{m}} - \boldsymbol{B}_{\mathrm{p}}\boldsymbol{\Gamma}_4\end{aligned} \tag{26}$$

where $\boldsymbol{\Gamma}_1 = \boldsymbol{G}_{\mathrm{e}}(t) - \boldsymbol{G}_{\mathrm{e}}(0)$, $\boldsymbol{\Gamma}_2 = \boldsymbol{G}_{\mathrm{m}}(t) - \boldsymbol{G}_{\mathrm{m}}(0)$, $\boldsymbol{\Gamma}_3 = \boldsymbol{G}_{\mathrm{f}}(t) - \boldsymbol{G}_{\mathrm{f}}(0)$, $\boldsymbol{\Gamma}_4 = \boldsymbol{G}_{\mathrm{d}}(t) - \boldsymbol{G}_{\mathrm{d}}(0)$.

Define a Lyapunov function V_{I} as

$$V_{\mathrm{I}} = \frac{1}{2}\left(\boldsymbol{e}_{\mathrm{I}}^{\mathrm{T}}\boldsymbol{P}_{\mathrm{I}}\boldsymbol{e}_{\mathrm{I}} + \sum_{i=1}^{3}\frac{\Delta_{l_i}^2}{\alpha_i} + \sum_{i=1}^{3}\frac{\Delta_{\bar{f}_{ai}}^2}{\beta_i} + \mathrm{tr}\left(\boldsymbol{\Gamma}_1^{\mathrm{T}}\boldsymbol{\Phi}_1\boldsymbol{\Gamma}_1 + \boldsymbol{\Gamma}_2^{\mathrm{T}}\boldsymbol{\Phi}_2\boldsymbol{\Gamma}_2 + \boldsymbol{\Gamma}_3^{\mathrm{T}}\boldsymbol{\Phi}_3\boldsymbol{\Gamma}_3 + \boldsymbol{\Gamma}_4^{\mathrm{T}}\boldsymbol{\Phi}_4\boldsymbol{\Gamma}_4\right)\right) \tag{27}$$

where $\boldsymbol{e}_{\mathrm{I}} = \left[\boldsymbol{e}_{\mathrm{po}}^{\mathrm{T}}, \boldsymbol{e}_{\mathrm{mp}}^{\mathrm{T}}\right]^{\mathrm{T}}$, $\boldsymbol{P}_{\mathrm{I}} = \mathrm{diag}\{\boldsymbol{P}_{\mathrm{po}}, \boldsymbol{P}_{\mathrm{mp}}\}$, $\boldsymbol{\Phi}_1$, $\boldsymbol{\Phi}_2$, $\boldsymbol{\Phi}_3$, and $\boldsymbol{\Phi}_4$ are positive definite symmetric matrices. $\alpha_i > 0$ and $\beta_i > 0$ are adaptation rates. The first derivative of V_{I} can be written as

$$\begin{aligned}\dot{V}_{\mathrm{I}} = {} & \frac{1}{2}\boldsymbol{e}_{\mathrm{po}}^{\mathrm{T}}\left(\boldsymbol{F}_{\mathrm{o}}^{\mathrm{T}}\boldsymbol{P}_{\mathrm{po}} + \boldsymbol{P}_{\mathrm{po}}\boldsymbol{F}_{\mathrm{o}}\right)\boldsymbol{e}_{\mathrm{po}} \\ & + \frac{1}{2}\boldsymbol{e}_{\mathrm{mp}}^{\mathrm{T}}\left(\boldsymbol{A}_{\mathrm{pH}}^{\mathrm{T}}\boldsymbol{P}_{\mathrm{mp}} + \boldsymbol{P}_{\mathrm{mp}}\boldsymbol{A}_{\mathrm{pH}}\right)\boldsymbol{e}_{\mathrm{mp}} \\ & + \boldsymbol{e}_{\mathrm{po}}^{\mathrm{T}}\boldsymbol{P}_{\mathrm{po}}\sum_{i=1}^{3}\boldsymbol{J}_{\mathrm{o}}\boldsymbol{b}_{\mathrm{p}i}\Delta_{l_i}\boldsymbol{u}_{\mathrm{p}i} + \boldsymbol{e}_{\mathrm{po}}^{\mathrm{T}}\boldsymbol{P}_{\mathrm{po}}\sum_{i=1}^{3}\boldsymbol{J}_{\mathrm{o}}\boldsymbol{b}_{\mathrm{p}i}\Delta_{\bar{f}_{ai}} \\ & - \boldsymbol{e}_{\mathrm{mp}}^{\mathrm{T}}\boldsymbol{P}_{\mathrm{mp}}\boldsymbol{B}_{\mathrm{p}}\boldsymbol{\Gamma}_1\boldsymbol{e}_{\mathrm{mp}} - \boldsymbol{e}_{\mathrm{mp}}^{\mathrm{T}}\boldsymbol{P}_{\mathrm{mp}}\boldsymbol{B}_{\mathrm{p}}\boldsymbol{\Gamma}_2\boldsymbol{x}_{\mathrm{m}} - \boldsymbol{e}_{\mathrm{mp}}^{\mathrm{T}}\boldsymbol{P}_{\mathrm{mp}}\boldsymbol{B}_{\mathrm{p}}\boldsymbol{\Gamma}_3\bar{\boldsymbol{f}}_{\mathrm{m}} \\ & - \boldsymbol{e}_{\mathrm{mp}}^{\mathrm{T}}\boldsymbol{P}_{\mathrm{mp}}\boldsymbol{B}_{\mathrm{p}}\boldsymbol{\Gamma}_4 - \sum_{i=1}^{3}\frac{\Delta_{l_i}}{\alpha_i}\dot{\hat{l}}_i - \sum_{i=1}^{3}\frac{\Delta_{\bar{f}_{ai}}}{\beta_i}\dot{\hat{\bar{f}}}_{ai} \\ & + \mathrm{tr}\left(\dot{\boldsymbol{G}}_{\mathrm{e}}^{\mathrm{T}}(t)\boldsymbol{\Phi}_1\boldsymbol{\Gamma}_1 + \dot{\boldsymbol{G}}_{\mathrm{m}}^{\mathrm{T}}(t)\boldsymbol{\Phi}_2\boldsymbol{\Gamma}_2 + \dot{\boldsymbol{G}}_{\mathrm{f}}^{\mathrm{T}}(t)\boldsymbol{\Phi}_3\boldsymbol{\Gamma}_3 + \dot{\boldsymbol{G}}_{\mathrm{d}}^{\mathrm{T}}(t)\boldsymbol{\Phi}_4\boldsymbol{\Gamma}_4\right)\end{aligned} \tag{28}$$

Choose appropriate matrices so that

$$\boldsymbol{e}_{\mathrm{po}}^{\mathrm{T}}\boldsymbol{P}_{\mathrm{po}}\sum_{i=1}^{3}\boldsymbol{J}_{\mathrm{o}}\boldsymbol{b}_{\mathrm{p}i}\Delta_{l_i}\boldsymbol{u}_{\mathrm{p}i} = \sum_{i=1}^{3}\frac{\Delta_{l_i}}{\alpha_i}\dot{\hat{l}}_i \tag{29}$$

$$\boldsymbol{e}_{\mathrm{po}}^{\mathrm{T}}\boldsymbol{P}_{\mathrm{po}}\sum_{i=1}^{3}\boldsymbol{J}_{\mathrm{o}}\boldsymbol{b}_{\mathrm{p}i}\Delta_{\bar{f}_{ai}} = \sum_{i=1}^{3}\frac{\Delta_{\bar{f}_{ai}}}{\beta_i}\dot{\hat{\bar{f}}}_{ai} \tag{30}$$

$$\boldsymbol{e}_{\mathrm{mp}}^{\mathrm{T}}\boldsymbol{P}_{\mathrm{mp}}\boldsymbol{B}_{\mathrm{p}}\boldsymbol{\Gamma}_1\boldsymbol{e}_{\mathrm{mp}} = \mathrm{tr}\left(\boldsymbol{G}_{\mathrm{e}}^{\mathrm{T}}(\mathrm{t})\boldsymbol{\Phi}_1\boldsymbol{\Gamma}_1\right) \tag{31}$$

$$\boldsymbol{e}_{\mathrm{mp}}^{\mathrm{T}}\boldsymbol{P}_{\mathrm{mp}}\boldsymbol{B}_{\mathrm{p}}\boldsymbol{\Gamma}_2\boldsymbol{x}_{\mathrm{m}} = \mathrm{tr}\left(\boldsymbol{G}_{\mathrm{m}}^{\mathrm{T}}(\mathrm{t})\boldsymbol{\Phi}_2\boldsymbol{\Gamma}_2\right) \tag{32}$$

$$\boldsymbol{e}_{\mathrm{mp}}^{\mathrm{T}}\boldsymbol{P}_{\mathrm{mp}}\boldsymbol{B}_{\mathrm{p}}\boldsymbol{\Gamma}_3\bar{\boldsymbol{f}}_{\mathrm{m}} = \mathrm{tr}\left(\boldsymbol{G}_{\mathrm{f}}^{\mathrm{T}}(\mathrm{t})\boldsymbol{\Phi}_3\boldsymbol{\Gamma}_3\right) \tag{33}$$

$$\boldsymbol{e}_{\mathrm{mp}}^{\mathrm{T}}\boldsymbol{P}_{\mathrm{mp}}\boldsymbol{B}_{\mathrm{p}}\boldsymbol{\Gamma}_4 = \mathrm{tr}\left(\boldsymbol{G}_{\mathrm{d}}^{\mathrm{T}}(\mathrm{t})\boldsymbol{\Phi}_4\boldsymbol{\Gamma}_4\right) \tag{34}$$

Then, the adaptive laws in Theorem 2 are got and Eq. (28) is rewritten as

$$\dot{V}_{\mathrm{I}} = \frac{1}{2}\left(\boldsymbol{e}_{\mathrm{po}}^{\mathrm{T}}\left(\boldsymbol{F}_{\mathrm{o}}^{\mathrm{T}}\boldsymbol{P}_{\mathrm{po}} + \boldsymbol{P}_{\mathrm{po}}\boldsymbol{F}_{\mathrm{o}}\right)\boldsymbol{e}_{\mathrm{po}} + \boldsymbol{e}_{\mathrm{mp}}^{\mathrm{T}}\left(\boldsymbol{A}_{\mathrm{pH}}^{\mathrm{T}}\boldsymbol{P}_{\mathrm{mp}} + \boldsymbol{P}_{\mathrm{mp}}\boldsymbol{A}_{\mathrm{pH}}\right)\boldsymbol{e}_{\mathrm{mp}}\right) \tag{35}$$

The designed $\boldsymbol{F}_{\mathrm{o}}$ and $\boldsymbol{A}_{\mathrm{pH}}$ are Hurwitz matrices, so that a positive definite symmetric matrix $\boldsymbol{Q}_{\mathrm{I}} = \mathrm{diag}\{\boldsymbol{Q}_{\mathrm{po}}, \boldsymbol{Q}_{\mathrm{mp}}\}$ satisfies the Lyapunov equation $\boldsymbol{F}_{\mathrm{o}}^{\mathrm{T}}\boldsymbol{P}_{\mathrm{po}} + \boldsymbol{A}_{\mathrm{pH}}^{\mathrm{T}}\boldsymbol{P}_{\mathrm{mp}} + \boldsymbol{P}_{\mathrm{po}}\boldsymbol{F}_{\mathrm{o}} + \boldsymbol{P}_{\mathrm{mp}}\boldsymbol{A}_{\mathrm{pH}} = -\boldsymbol{Q}_{\mathrm{I}}$, i.e., $\dot{V}_{\mathrm{I}} < 0$. Moreover, $V_{\mathrm{I}}(t) > 0$ holds based on Eq. (27). This completes the proof.

Remark 3. *The key for achieving stable fault-tolerant control design is to run the system with the fault estimation in the loop, use these estimate values in the control law, and adjust them in a way which assures the overall closed-loop system stability. It is the motivation for the proposed integration scheme. Moreover, there are many aeroelastic mode states in the GRA model and they cannot be measured by sensors directly, so that an output feedback control method based on the observer is utilized here.*

5. Simulation results

In this section, the integrated method (FTC) is compared with a Static Output Feedback (SOF) proposed in Ref. 2 and the

Open-Loop (OL). Four scenarios are used to compare the performance of FTC. This simulation analysis concentrates on the flight maneuvering stability and mitigation of gust loading of the GRA model. The flight condition is shown in Table. 2.

In the GRA model, the number of rigid variables for the longitudinal plane is 3 and the number of modes $\boldsymbol{\eta}$ is 22 for zero-fuel weight. $\boldsymbol{B}_g\boldsymbol{w}_g$ and $\boldsymbol{D}_g\boldsymbol{w}_g$ (in which the sensor noises are considered) are calculated and provided by the Alenia Aermacchi. The surfaces for control contain right-hand outboard aileron δ_{roa}, left-hand outboard aileron δ_{loa}, right-hand inboard aileron δ_{ria}, left-hand inboard aileron δ_{lia}, right-hand elevator δ_{re}, and left-hand elevator δ_{le}. Since GRA is a symmetric model, only δ_{roa}, δ_{ria}, and δ_{re} are considered to design the controller. It is important to underline that, to obtain a symmetric rotation of aileron control surfaces, a positive rotation must be assigned to the right aileron and a negative one to the left one, and vice versa. The control surface amplitude saturation is $\pm30(°)$ and the surface rate limiting is $\pm80(°)$. The detailed system outputs are reported in Table. 3, where IMU signals are taken near to the center of gravity of the aircraft, the feed-forward sensor is positioned on the nose of the aircraft, and the right wing is the wing tip grid on the front spar.

Table 2 Flight condition.

Property	Value
Aircraft velocity	$V_a = 241.4$ (m/s)
Flight height	$h = 8000$ m
Dynamic pressure	$p_a = 12826$ Pa
Gust frequency	$f_g = 3.41$ Hz
Gust wavelength	$L_g = 47.9$ m
Gust velocity	$w_{g0} = 12.845$ (m/s)

Table 3 Description for system outputs.

No.	Position	Property	Symbol
1	IMU	Displacement in z direction	z (m)
2	IMU	Pitch angle	θ (°)
3	IMU	Pitch rate	q ((°)/s)
4	IMU	Angle of attack	α (°)
5	IMU	Acceleration in z direction	a_z (m/s^2)
6	IMU	Load factor	n_z (g)
7	Right wing-tip	Displacement in z direction	z_{wing} (m)
8	Right wing-tip	Pitch angle	θ_{wing} (deg)
9	Right wing-tip	Acceleration in z direction	$a_{z,wing}$ (m/s^2)
10	Feed-forward sensor	Angle of attack	α_{nose} (°)

5.1. Simulation of normal case

In this case, the control surfaces δ_{roa}, δ_{ria}, and δ_{re} are considered without actuator faults. The reference signal is given as

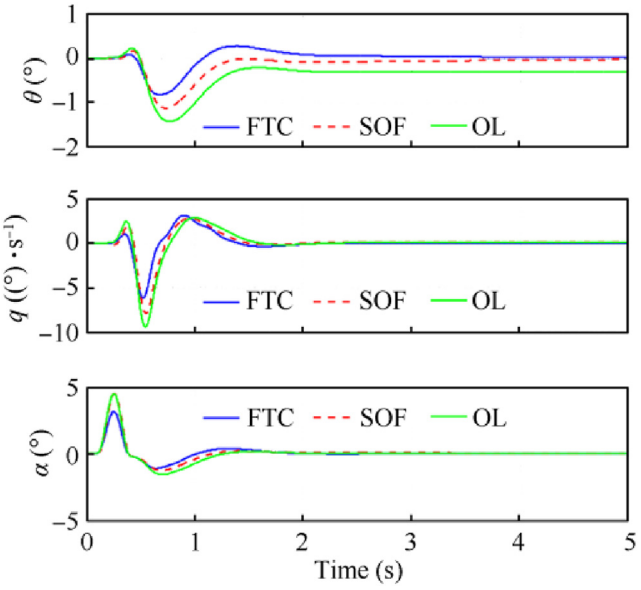

Fig. 3 Flight maneuver for GRA in normal case.

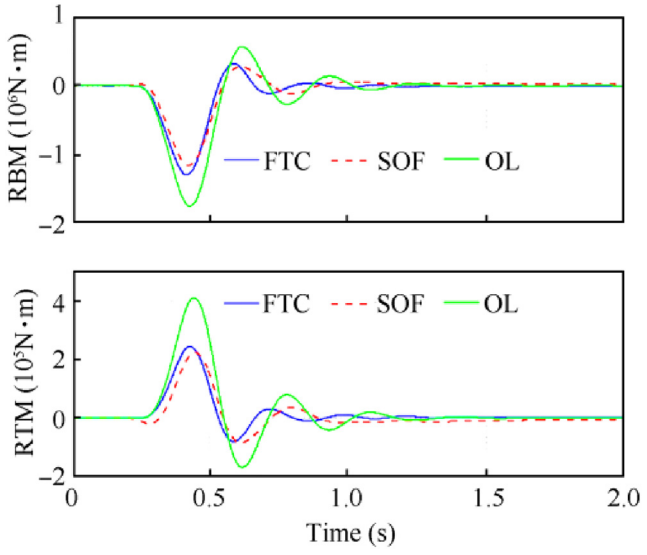

Fig. 2 Wing loads for GRA in normal case.

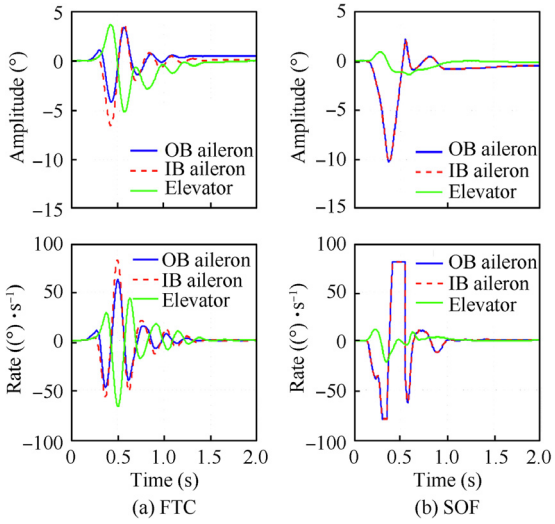

Fig. 4 Amplitude and rate of surfaces in normal case.

$\boldsymbol{r} = [\theta_r, \alpha_r]^T$, where $\theta_r = 0^\circ$ denotes the reference pitch angle and $\alpha_r = 0^\circ$ is the reference attack angle.

Wing loads obtained in the normal case are displayed in Fig. 2, showing that both FTC and SOF reduce the bending moment and torsional moment effectively than the open-loop. The peak values of the moments between FTC and SOF are nearly the same. Fig. 3 compares the longitudinal closed-loop responses (pitch angle, pitch angle rate, and attack angle) obtained by FTC with these obtained by SOF. As it can be seen, both FTC and SOF can effectively control the attitude of the aircraft. From Fig. 4, it confirms that the deflections of these surfaces always work below their allowed actuator saturations with FTC. However, the deflection rates of these three surfaces reach their rate limit with SOF. It can be concluded from Figs. 2 and 3 that the SOF controller works well by its robustness even if the actuators meet saturations.

5.2. Simulation of LOE fault

In this case, δ_{roa}, δ_{ria}, and δ_{re} are again modeled, this time with a 50% loss of the δ_{roa} effectiveness, i.e., $l_1 = 0.5$, $\bar{l}_1 = -0.5$. As before $\boldsymbol{r} = [\theta_r, \alpha_r]^T$, where $\theta_r = 0^\circ$ and $\alpha_r = 0^\circ$.

Moments on the wing root obtained in the LOE case are displayed in Fig. 5. The peak values of them show that FTC is capable of a slightly better moment reduction than the SOF controller. Fig. 6 compares the longitudinal closed-loop responses obtained by FTC with those obtained by SOF. Both FTC and SOF control the attitude of aircraft, effectively.

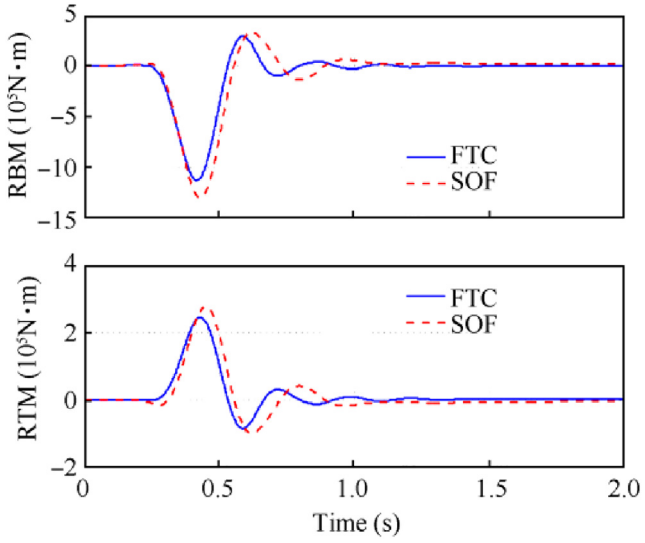

Fig. 5 Wing loads for GRA in LOE case.

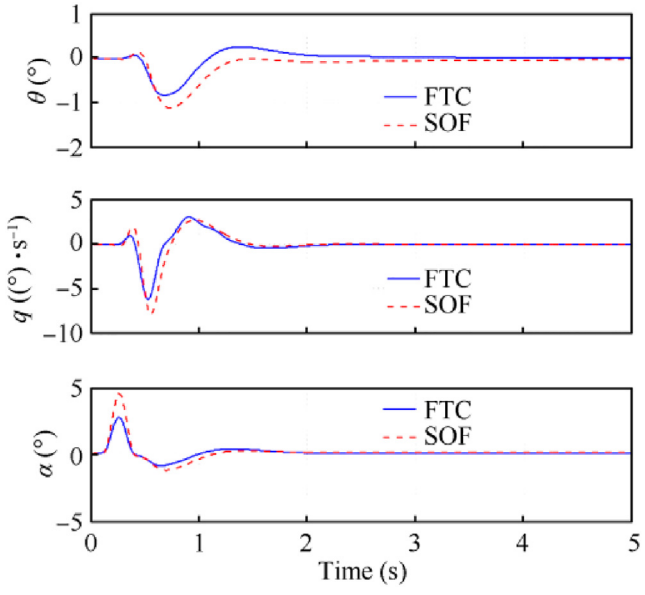

Fig. 6 Flight maneuver for GRA in LOE case.

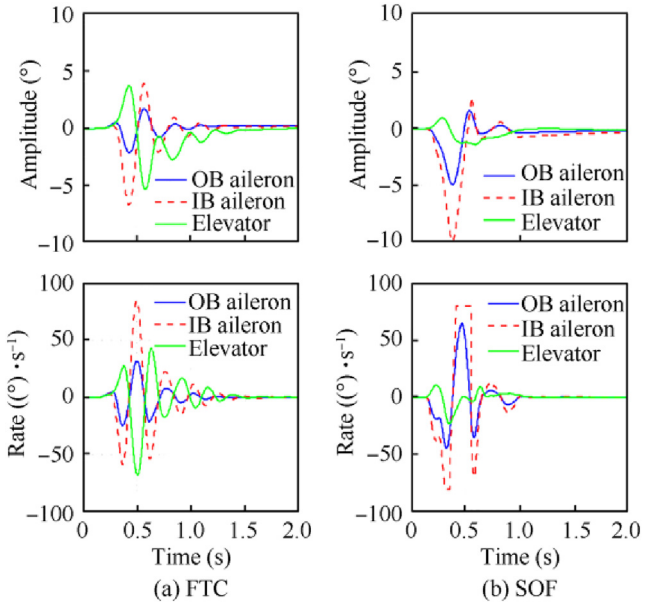

Fig. 7 Amplitude and rate of surfaces in LOE case.

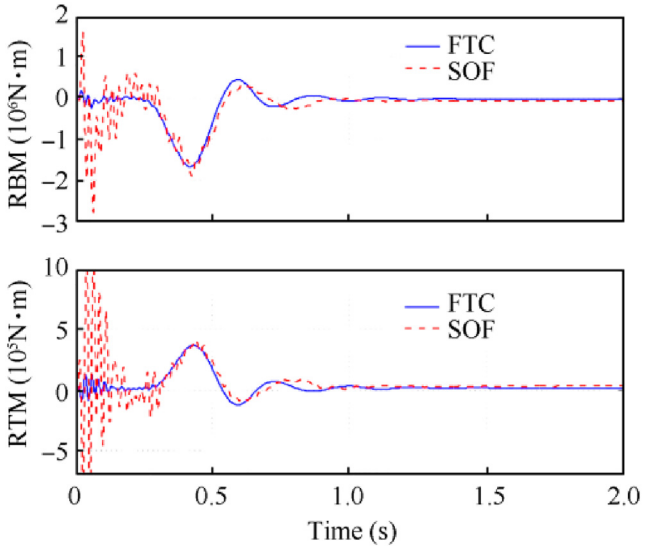

Fig. 8 Wing loads for GRA in LIP case.

Fig. 7 shows the comparison of the surface deflection amplitudes and rates between FTC and SOF. In the LOE case, the fault actuator moves slowly when a control command is injected into it. This reduces the control performance (the moment peak value in Fig. 2 is less than the one in Fig. 5) but does not generate additional structural loads.

5.3. Simulation of LIP fault

In this case, the actuator δ_{roa} is locking at a 5° deflection during the whole simulation. $\boldsymbol{r} = [\theta_r, \alpha_r]^T$, $\theta_r = 0^\circ$, $\alpha_r = 0^\circ$.

Fig. 8 shows wing loads obtained in the LIP case. The load alleviation is achieved using FTC and the fault actuator just slightly affects the structural load when injecting the LIP fault into the actuator. However, SOF cannot reduce moments effectively and the oscillations caused by fault have a significant influence on structural loads. Fig. 9 compares the longitudinal closed-loop responses obtained by FTC with those obtained by SOF. FTC can control the attitude of aircraft effectively but the pitch angle cannot be re-stabilized to zero by using SOF. Comparisons of surface deflection amplitudes and rates of the closed-loop system using FTC and SOF controller are shown in Fig. 10. When δ_{roa} locks in 5°, δ_{ria} (calculated by FTC) compensates the additional moment caused by δ_{roa}, whereas δ_{ria} (calculated by SOF) cannot. δ_{roa} and δ_{ria} (calculated by SOF) are both positive, which explains why the pitch angle does not equal to zero after the system re-stabilize by using SOF.

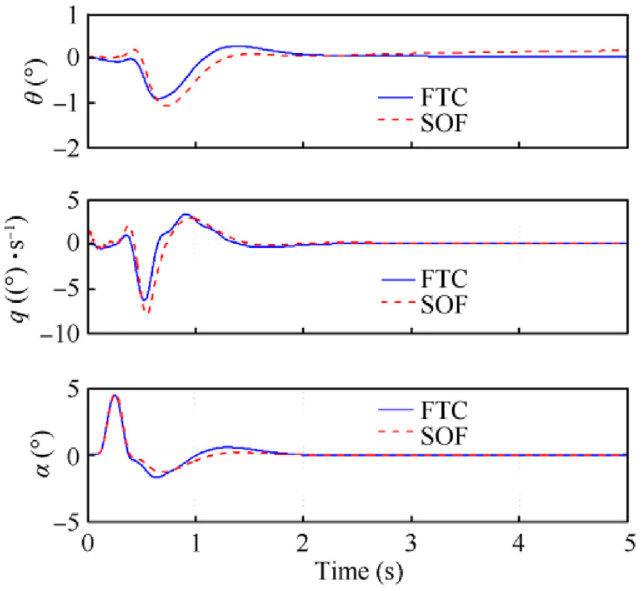

Fig. 9 Flight maneuver for GRA in LIP case.

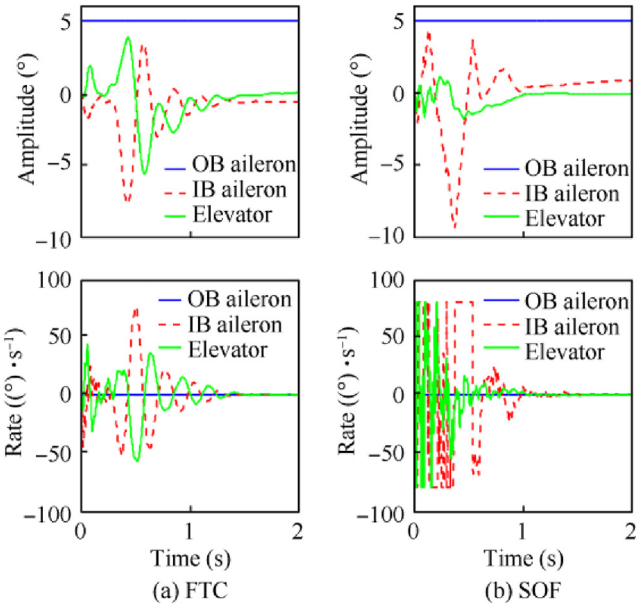

Fig. 10 Amplitude and rate of surfaces in LIP case.

5.4. Simulation of OFC

In this final simulation case, a 'solid' OFC signal with amplitude of 2° and frequency of 7 Hz is employed to compare the performances of FTC and SOF. $\boldsymbol{r} = [\theta_r, \alpha_r]^T$, $\theta_r = 0^\circ$, $\alpha_r = 0^\circ$.

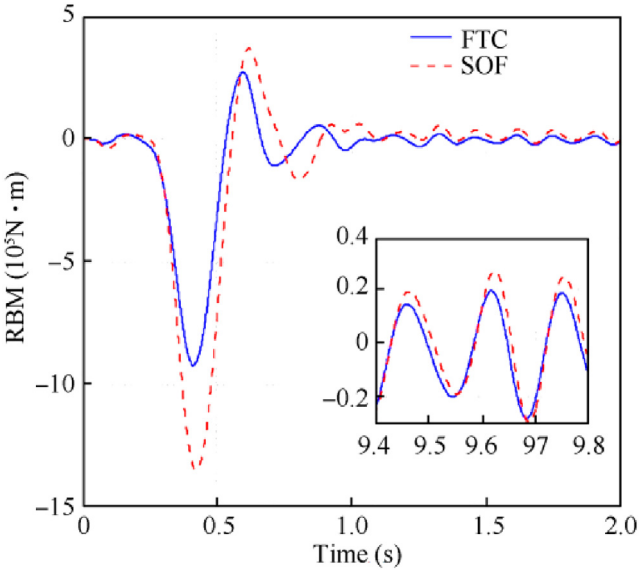

Fig. 11 Bending moment for GRA in OFC.

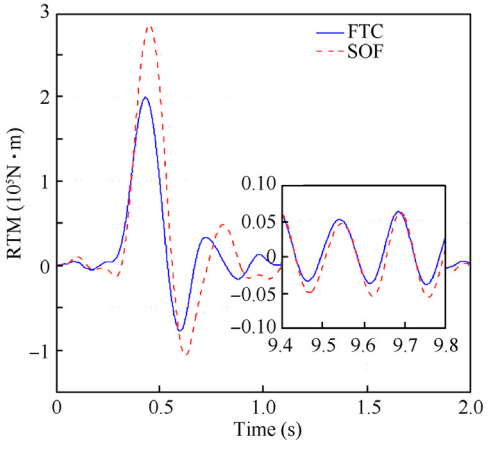

Fig. 12 Torsional moment for GRA in OFC.

Figs. 11 and 12 show structure loads obtained in OFC. Compared with the SOF controller, FTC provides a higher bending moment reduction (see the peak values). Although the oscillation cannot be fully eliminated, FTC reduces their bending moment amplitude once the closed-loop system has re-stabilized. We can get the same result from the simulation of the torsional moment. Fig. 13 shows that both FTC and SOF regulate the attitude of aircraft effectively. The amplitudes and rates of the actuators for the post-fault system are shown in Fig. 14.

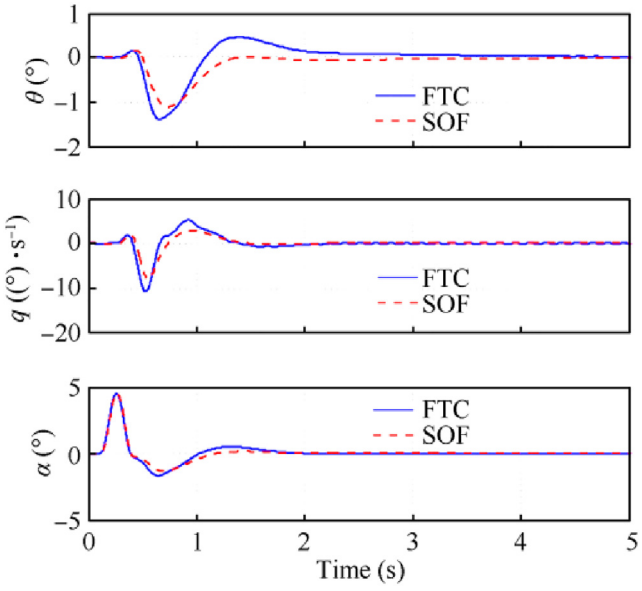

Fig. 13 Flight maneuver for GRA in OFC.

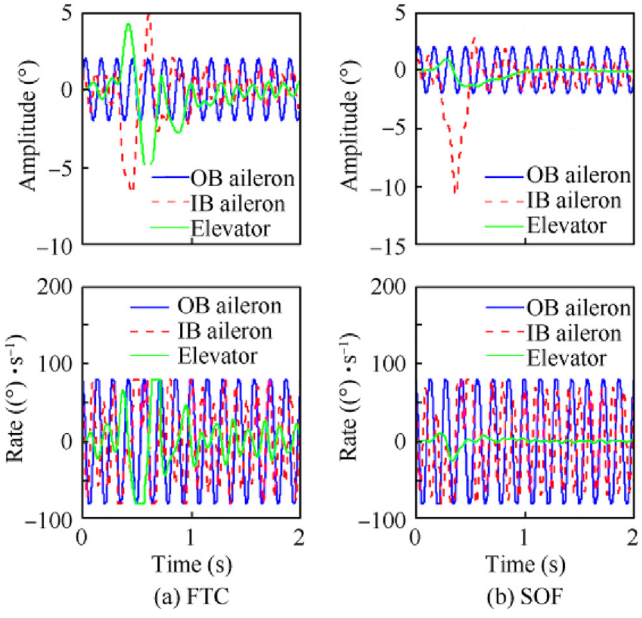

Fig. 14 Amplitude and rate of surfaces in OFC.

6. Conclusions

(1) The proposed novel integration strategy cannot only overcome the pairing between the rigid body and the elastic mode, but also deal with the interaction between the fault estimation and the reconfigurable control.
(2) Simulation results are presented for a variety of actuator fault cases and their performances are assessed by the reduction of generated gust loads. It can be concluded that the designed integrated controller mitigates the effect of gust loading and has better fault-tolerant performance than the reference static output feedback controller.
(3) It can also be concluded that the lock-in-place and oscillatory failure case, which generate external moment on wings and cause undesired oscillation, are more serious than the loss-of-effectiveness. These unexpected loads may cause the actuator saturation which will be investigated in our future work.

Declaration of Competing Interest

The authors declare that they have no known competing financial interests or personal relationships that could have appeared to influence the work reported in this paper.

Acknowledgements

The work reported in this paper is supported by the National Key Research and Development Plan of China (No. 2019YFB1706001) and the National Natural Science Foundation of China (No. 61773001).

References

1. Regan CD, Jutte CV. Survey of applications of active control technology for gust alleviation and new challenges for lighter-weight aircraft. Washington, D.C.: NASA; 2000, Report No.: NASA/TM-2012-216008.
2. Fonte F, Ricci S, Mantegazza P. Gust load alleviation for a regional aircraft through a static output feedback. *J Aircr* 2015;**52**(5):1559–74.
3. Howcroft C, Calderon D, Cooper JE, et al. Gust alleviation of a simulated regional jet model using multiple control surfaces. *International forum on aeroelasticity and structural dynamics*, 2015.
4. Haghighat S, Liu HHT, Martins JRRA. Model-predictive gust load alleviation controller for a highly flexible aircraft. *J Guid Control Dyn* 2012;**35**(6):1751–66.
5. Fan W, Liu HH, Kwong R. The influence of control surface faults on flexible aircraft. *AIAA guidance, navigation, and control conference*; 2016.
6. Fan W, Liu HH, Kwong R. Gust load alleviation control for a flexible aircraft with loss of control effectiveness. *AIAA guidance, Navigation, and Control Conference*. 2017.
7. Fan W, Liu HHT, Kwong RHS. Gain-scheduling control of flexible aircraft with actuator saturation and stuck faults. *J Guid Control Dyn* 2017;**40**(3):510–20.
8. Goupil P. Oscillatory failure case detection in the A380 electrical flight control system by analytical redundancy. *Control Eng Pract* 2010;**18**(9):1110–9.
9. Liu Y, Dong X, Ren Z, et al. Fault-tolerant control for commercial aircraft with actuator faults and constraints. *J Frankl Inst* 2019;**356**(7):3849–68.

10. Wang J, Wang S, Wang X, et al. Active fault tolerant control for vertical tail damaged aircraft with dissimilar redundant actuation system. *Chin J Aeronaut* 2016;**29**(5):1313–25.
11. Wang X, Wang S, Yang Z, et al. Active fault-tolerant control strategy of large civil aircraft under elevator failures. *Chin J Aeronaut* 2015;**28**(6):1658–66.
12. Hong S, Yue T, Liu H. Vehicle energy system active defense: a health assessment of lithium-ion batteries. *Int J Intell Syst* 2020; https://doi.org/10.1002/int.22309.
13. Hong S, Zeng Y. A health assessment framework of lithium-ion batteries for cyber defense. *Appl Soft Comput* 2021;**101**: 107067.
14. Hong S, Lv C, Zhao T, et al. Cascading failure analysis and restoration strategy in an interdependent network. *J Phys A: Math Theor* 2016;**49**(19):195101.
15. Hong S, Zhu J, Braunstein LA, et al. Cascading failure and recovery of spatially interdependent networks. *J Stat Mech* 2017;**2017**(10):103208.
16. Lu P, van Kampen EJ, de Visser C, et al. Aircraft fault-tolerant trajectory control using incremental nonlinear dynamic inversion. *Control Eng Pract* 2016;**57**:126–41.
17. Li Q, Yang H, Zhao D, Jiang B. Fault-tolerant control and vibration suppression of flexible spacecraft: An interconnected system approach. *Chin J Aeronaut* 2020;**33**(7):2014–23.
18. Ding SX. Integrated design of feedback controllers and fault detectors. *Annu Rev Control* 2009;**33**(2):124–35.
19. Qi F, Ma Y. Integrated fault estimation and fault-tolerant control for uncertain time-varying delay nonlinear Markovian jump systems. *Int J Robust Nonlinear Control* 2018;**28**(18):5766–85.
20. Gao Z, Ding SX. Actuator fault robust estimation and fault-tolerant control for a class of nonlinear descriptor systems. *Automatica* 2007;**43**(5):912–20.
21. Han J, Zhang H, Wang Y, et al. Disturbance observer based fault estimation and dynamic output feedback fault tolerant control for fuzzy systems with local nonlinear models. *ISA Trans* 2015;**59**:114–24.
22. Qian H, Peng Y, Yang G. Reduced-order observer-based fault estimation and fault-tolerant control for a class of discrete Lipschitz nonlinear systems. *Optim Control Appl Meth* 2016;**37** (6):1236–62.
23. Liu Y, Ren Z, Cooper JE. Integrated strategy for commercial aircraft fault-tolerant control. *J Guid Control Dyn* 2018;**41** (6):1423–34.
24. Wang T, Wang J, Wu Y, et al. A fault diagnosis model based on weighted extension neural network for turbo-generator sets on small samples with noise. *Chin J Aeronaut* 2020;**33**(10):2757–69.
25. Ma Z, Wang S, Shi J, et al. Fault diagnosis of an intelligent hydraulic pump based on a nonlinear unknown input observer. *Chin J Aeronaut* 2018;**31**(2):385–94.
26. Zhang C, Liu Y, Wan F, et al. Multi-faults diagnosis of rolling bearings via adaptive customization of flexible analytical wavelet bases. *Chin J Aeronaut* 2020;**33**(2):407–17.
27. Roskam J. *Airplane flight dynamics and automatic flight controls*. Kansas: Lawrence; 2001.
28. Wright JR, Cooper JE. *Introduction to aircraft aeroelasticity and loads*. Chichester, UK: John Wiley & Sons Ltd; 2014.
29. Chen J, Patton RJ, Zhang HY. Design of unknown input observers and robust fault detection filters. *Int J Control* 1996;**63** (1):85–105.